Results in Earth Sciences 4 (2026) 100163

Contents lists available at ScienceDirect

Results in Earth Sciences

journal homepage: www.sciencedirect.com/journal/results-in-earth-sciences

Characterization of gangue minerals in graphite from the Bahia-Minas Graphite Province, Brazil

David Currie [a,*], Francisco Teixeira Vilela [b], Débora Rabelo Matos [c], Joanna Chaves Souto Araújo [b]

[a] British Geological Survey, The Lyell Centre, Research Avenue South, Edinburgh EH14 4AP, UK
[b] Serviço Geológico do Brasil, Avenida Brasil, 1731, Bairro Funcionários, Belo Horizonte, MG 30140-002, Brazil
[c] Serviço Geológico do Brasil, ERJ (Escritório do Rio de Janeiro) Avenida Pasteur, 404 – Urca, Rio de Janeiro, RJ 22290-255, Brazil

ARTICLE INFO

Keywords:
Graphite
Brazil
SEM
Critical Minerals
Mineralogy
Petrology
Characterization

ABSTRACT

Natural graphite is a chemically inert, non-toxic mineral with exceptional thermal and electrical properties, making it critical for electronics, steelmaking, and lithium-ion batteries. Brazil hosts significant flake, vein, and amorphous graphite deposits and is a top-four producer of graphite. This study examines gangue mineral inclusions in graphite from the Bahia-Minas Graphite Province (BMGP), Brazil's main graphite-producing region. Graphite occurs within paragneiss and schist of the Jequitinhonha Complex and Macaúbas Group, formed under medium- to high-grade metamorphism. Using scanning electron microscopy (SEM), energy dispersive X-ray spectroscopy, and in-lens secondary electron imaging, we characterize mineral assemblages and microtextural relationships between graphite and gangue phases to better understand the mineralogy and morphology of gangue mineral impurities, which may cause issues with mineral processing at a later stage. Fourteen samples reveal graphite-bearing rocks with gneissose and mylonitic textures. Kaolinite and quartz dominate gangue minerals within graphite cleavages and interstitial zones, alongside K-feldspar, jarosite, tourmaline, and sillimanite. Sillimanite and biotite confirm amphibolite-facies metamorphism, while kaolinite, smectite, and jarosite indicate retrograde alteration and low-temperature fluid infiltration. Jarosite reflects post-peak oxidation of iron sulfides under acidic conditions, marking supergene weathering or hydrothermal overprinting. In-lens SEM imaging shows stacked graphite flakes intercalated with gangue minerals. Quartz and K-feldspar exhibit mechanically entrapped morphologies, whereas kaolinite appears intergrown, suggesting early diagenetic incorporation or retrograde origin. These observations align with impurity classification models and underscore graphite's structural sensitivity to processing. Linking gangue morphology and graphite texture informs beneficiation strategies to preserve graphite integrity and refines mineral systems models for BMGP and analogous terranes.

1. Introduction

Natural graphite ('graphite' herein) is chemically inert and non-toxic and has a unique combination of physical properties including high electrical conductivity, a high melting point, resistance to corrosion, and lubricity. It is primarily found in metamorphic rocks, where it forms through the metamorphism of organic-rich sediments or carbonaceous material (Luque et al., 2014; Robinson et al., 2017; Pacheco et al., 2021). Graphite deposits of economic interest are grouped into two broad categories: amorphous (microcrystalline) and crystalline (flake, vein, lump, or chip). Flake graphite, which is the focus of this study, occurs as isolated, flat, plate-like particles with hexagonal edges, often found in medium- to higher-grade regional metamorphic rocks such as schists and gneisses, respectively. Vein graphite, also known as lump graphite, forms in veins or fractures within metamorphic and igneous rocks, characterized by its high purity and crystalline nature (Luque et al., 2014; Simandl et al., 2015). Amorphous or microcrystalline graphite is primarily extracted from heat-affected coal beds and appears as fine to nanoscale particles (Robinson et al., 2017).

These unique properties have led to graphite use in multiple industrial applications in electronics, lubrication, steel production, and aviation, and as the anode material in lithium-ion battery technologies

* Corresponding author.
E-mail address: dcur@bgs.ac.uk (D. Currie).

https://doi.org/10.1016/j.rines.2026.100163
Received 12 February 2026; Received in revised form 2 June 2026; Accepted 2 June 2026
Available online 3 June 2026
2211-7148/© 2026 The Author(s). Published by Elsevier Inc. This is an open access article under the CC BY license (http://creativecommons.org/licenses/by/4.0/).

(Jara et al., 2019). Since 2020, global graphite production (amorphous and flake, but excluding synthetic) has increased by over 20% from 1.4 million tonnes (Mt) to 1.7 Mt (Idoine et al., 2026). In 2024, China is estimated to have produced over 74% (1.27 Mt) of global natural graphite. From 2022–2024, output from Brazil declined by over 18% from around 80 kilotonnes (Kt) to 65 Kt. (Idoine et al., 2026). China holds the world's largest reserves of graphite with around 100Mt while Brazil ranks second with reserves of around 74Mt (U.S. Geological Survey, 2026).

Global demand for graphite is expected to double by 2030 and increase fivefold by 2050 (IEA, 2024). This is predominantly driven by the expansion of the battery industry as economies progress towards greenhouse gas emission reduction targets (Hund et al., 2023; IEA, 2024). Since China produces over 90% of the final processed material needed for battery anodes and is likely to control supply for the foreseeable future, diversification of the graphite supply chain is already a recurring geopolitical issue (Park et al., 2025). The resultant global supply risk associated with graphite and its economic importance in the electric vehicle market, for example, has led to graphite being listed as a critical mineral by the UK, EU, Canada, and Australia (Mudd et al., 2024). In Brazil, graphite is listed as a category 2 strategic mineral, meaning that it is important for use in high-tech products and processes (Pope and Smith, 2023).

As the demand for graphite is expected to rise in the coming decades, lower-grade deposits will likely be explored for development. Given the high energy and cost demands associated with multi-step beneficiation of graphitic raw material, it is essential to thoroughly characterize the raw material beforehand to enhance the efficiency of the beneficiation process and optimize the mineral processing chain. Graphite ore is currently characterized using a variety of techniques, including optical microscopy, X-ray powder diffraction (XRD), X-ray fluorescence (XRF), differential thermal analysis/thermogravimetry mass spectrometry (DTA/TGA-MS), Raman spectroscopy, secondary ion mass spectrometry (SIMS), automated mineral liberation analysis, and chemical analysis (Farquhar et al., 1999; Li et al., 2007; Natarajan et al., 2010; Sandmann et al., 2014; Popova, 2017; Jara et al., 2019, 2020; Li et al., 2021). Optical microscopy is the only one of these methods that can inform intermineral relationships and provide visual data related to impurity and or gangue mineral inclusions associated with the graphitic ore (Sandmann et al., 2014). However, optical microscopy and automated mineral liberation analysis fail to recognize the chemical and morphological characteristics of potentially submicron material routinely observed and assessed using scanning electron microscopy (SEM), in-lens secondary electron (SE), and energy dispersive X-ray (EDX) analysis.

The size and grade of graphite flakes are important parameters for the commercial viability and end uses of graphite. Reduction in flake size will lead to a reduction in product price (Jara et al., 2019). Reduction of grade will result in the graphite being used in less specialized and lower-priced end-use applications (Mitchell, 1992; Kim et al., 2003; Jara et al., 2019). Thus, minimizing the degree of crushing and milling and understanding the liberation characteristics and impurities of graphite is crucial (Sandmann et al., 2014; Chehreh Chelgani et al., 2016).

Flake graphite typically exhibits a layered structure, with significant cleavage parallel to these layers. The properties along the layers differ markedly from those perpendicular to them. Within the monoatomic layers, carbon atoms are bonded strongly through covalent bonds, while the layers themselves are held together by weak van der Waals bonds (Chehreh Chelgani et al., 2016). In the graphite structure, gangue minerals can be found between layers, stacks, or clusters. These impurities can either be mechanically attached to the surface of graphite flakes or intercalated between adjacent flakes. The composition of these impurities is suggested to be an important factor relating to the degree of graphite crystallinity.

Four types of gangue mineral impurity inclusions have been described by Kim et al. (2003) as follows:

- type 1: simple substance between graphite clusters, typically quartz, which can be removed by weak mechanical impact
- type 2: small, microtextured substance between graphite clusters, which is typically more mineralogically complex and strongly bound to the graphite cluster surface
- type 3: microtextured impurity substances that adhere and tangle strongly and widely, over and onto graphite cluster surfaces
- type 4: flat impurities sandwiched between graphite stacks within a cluster; the impurity has microtextured morphology and seems to provide strong binding to the graphite surface

The composition of types 1 and 2 were found to be more likely to result in higher crystallinity of graphite clusters than types 3 and 4. Simple mechanical impact testing of expanded graphite with type 1 inclusions resulted in 99.9% carbon content compared to 99.0% in expanded graphite with type 3 inclusions (Kim et al., 2003). Therefore, understanding the distribution and composition of impurity types and how best to process the graphite to avoid overgrinding can result in larger final flake size, increased product grade, and increased recovery (Chehreh Chelgani et al., 2016).

Using samples from Brazil's primary graphite-producing area, the Bahia-Minas Graphite Province (BMGP), this study uses SEM in parallel with EDX and in-lens SE detector SEM imaging (simply 'in-lens' hereafter) to characterize gangue mineral impurity inclusions associated with graphite. By carrying out this research, a better understanding of gangue mineral morphology and liberation methods is gained, which may help increase final product flake size and grade of graphite across the BMGP region and similar deposits globally. The mineralogy and petrology presented here could also be used to better inform graphite mineral systems approach exploration models.

2. Graphite in the Bahia-Minas Gerais Graphite Province (BMGP)

Brazil is among the world's major graphite producers and exporters, driven by increasing global demand related to steelmaking, energy storage, and high-technology applications (Sousa and Matos, 2020; Idoine et al., 2026). Most Brazilian graphite production is concentrated in the Bahia–Minas Gerais Graphite Province (BMGP), located in northeastern Minas Gerais and southern Bahia. The province hosts several large graphite deposits and active mines, including Salto da Divisa and Pedra Azul, operated by Nacional de Grafite Ltd. The Salto da Divisa deposit alone contains estimated resources of approximately 230 Mt grading around 25% carbon (Serviço Geológico do Brasil (SGB), 2026).

Graphite mineralization In the BMGP is associated with metasedimentary rocks metamorphosed during the Neoproterozoic evolution of the Araçuaí Orogen. Regional metamorphism during the Brasiliano orogeny promoted the transformation of organic-rich sedimentary material into crystalline graphite. The deposits occur mainly in two Proterozoic units: (i) graphite-bearing schists of the Macaúbas Group and (ii) graphite-rich paragneisses of the Jequitinhonha Complex (Pedrosa-Soares et al., 2011; Pacheco et al., 2021).

The Macaúbas Group represents a sedimentary succession deposited between ca. 900 and 660 Ma and later metamorphosed under greenschist-facies conditions. In this unit, graphite mineralization is hosted predominantly by graphite schists. In contrast, the Jequitinhonha Complex comprises aluminous paragneisses, quartzites, sillimanite-bearing rocks, and calc-silicate lenses metamorphosed under upper amphibolite- to granulite-facies conditions between ca. 580 and 545 Ma (Pedrosa-Soares et al., 2011; Pacheco et al., 2021). Graphite mineralization in this complex is typically associated with sillimanite–graphite paragneisses.

The Jequitinhonha Complex has been interpreted as part of the distal passive margin of the precursor basin of the Araçuaí Orogen, with

sedimentation of the protoliths likely occurring during the Cryogenian period (720–635 Ma) (Pedrosa-Soares et al., 2011; Gonçalves-Dias et al., 2011, 2016). Graphite occurs mainly as disseminated flakes within metamorphic host rocks, although locally massive vein-type mineralization is also present (Belém, 2006).

Previous studies indicate that graphite from the Macaúbas Group ranges from fine flake to jumbo flake, whereas graphite from the Jequitinhonha Complex ranges from fine flake to super jumbo in size (Belém, 2006). This wide variability in graphite flake size contributes to the potential use of BMGP graphite in a range of industrial and high-technology applications, including energy storage, electronics, aerospace, and other specialized sectors (Jara et al., 2019). The largest operating mines in the BMPG, including Salto da Divisa and Pedra Azul, exploit graphite hosted by the Jequitinhonha Complex, whereas the Maiquinique mine extracts fine-grained graphite from the Macaúbas Group.

3. Sampling and methodology

Fourteen samples were collected from multiple field excursions carried out by Geological Survey of Brazil (SGB) staff, including ten collected during a collaborative one-week field trip between the British Geological Survey (BGS) and SGB staff (all authors of this study) across the BMGP in March of 2024 (Table 1; Fig. 1) (Currie et al., 2024). All 30 μm thickness thin sections were prepared by SGB. SEM was carried out at the BGS Keyworth site by authors Currie and Vilela as part of a knowledge exchange visit from Vilela to BGS in August of 2024 and in-lens analysis by Currie in June of 2025.

SEM analyses were made using a Zeiss Sigma 300 VP-FEG with Bruker Quantax XFlash 6|30 Energy Dispersive X-Ray (EDX) detectors running with Bruker's Esprit software (V 2.5). The EDX system can detect elements from atomic number 5 (boron) to atomic number 92 (uranium) and has detection limits of the order of 0.2–0.5 wt% for most elements. For this study, the operating conditions for back scatter electron (BSE) and EDX analyses were between 15 and 20 kV accelerating voltage at an optimum working distance of between 8.5 and 10 mm with a 120 μm aperture in 'beam boost' mode, giving a nominal beam current of around 10 nA.system. Samples were analysed in the form of carbon sputter coated (≈25 nm thick) polished thin sections. The SEM was operated under conditions of high vacuum (1.2×10^{-6} Torr) at accelerating voltages ranging from 3 to 15 kV, with 8.5 mm optimal analytical working distance and an X-ray detector take-off angle of 35°. Quantitative analysis was not undertaken due to analytical challenges associated with the fine grain size and beam-sensitive nature of the experimental materials.

High-resolution imagery was performed at low kV (around 5 kV) at an optimum working distance of around 5–7 mm and using an in-lens SE detector. In-lens microscopy in SEM uses detectors integrated within the objective lens to collect high-resolution secondary electrons at low accelerating voltages. This design enhances surface sensitivity, reduces charging, and improves image quality for delicate or nanostructured samples, making it ideal for materials science, semiconductor analysis, biological imaging or, in the case of this study, nanoscale intercalants in graphite mineralization (Salzmann et al., 2024)

4. Results

4.1. SEM-EDX

Of the fourteen samples collected, the following seven representative samples were analysed using SEM:

- FV-R−059B
- EM-R−060
- FV-R−005B
- FV-R−209A
- FV-R−003B
- FV-R−212
- FV-R−024E

Of these seven samples, one (EM-R−060) is a graphite schist and the other six are of graphite-rich gneiss (Fig. 3). At the macroscopic or outcrop scale, the raw material is often heavily weathered and oxidized, coated with dust and road debris, and, at times, overgrown by vegetation (Fig. 2). The outcrops, once cleaned off and exposed, have mylonitic schistose texture at FV-R−024D and FV-R−024E (Fig. 2a, b). All other location outcrops, again once cleaned off and exposed, reveal gneissose banding with darker mafic, biotite-rich bands adjacent to grey, graphite-rich bands and boudinaged, leucosomal quartzofeldspathic bands (Fig. 2c, d, e). Graphite in all samples is crystalline flake graphite and ranges in long axis length from submicron to more than 1 mm but tends to be more commonly within the range of 'fine flake to jumbo' size fractions (106–500 μm) based on the classification in Jara et al. (2019).

Twelve of the samples can be described broadly as graphite-rich paragneiss with minor variation or as either mylonitic graphite-rich schist or biotite-graphite schist in one location (FV-R−024D and E). Differences in the gneissose material are primarily related to modal mineralogy and the occurrence of accessory mineral phases like sillimanite, tourmaline, and rutile (Figs. 2, 3, 4).

Results from BSE and EDX analyses show kaolinite to be the main gangue mineral present within flake graphite cleavages or in asperities related to flake graphite across the sample set. Quartz grains are commonly found as gangue minerals within cleavages of graphite, but to a lesser extent than kaolinite. Smectite-group clays, tourmaline, sillimanite, K-feldspar, albite, plagioclase, zircon, xenotime, jarosite, Fe-oxides, Ti-oxides, Fe-sulfides, and rutile are also present within flake graphite cleavages or in asperities related to flake graphite, but are less common than kaolinite and quartz. In sample FV-R−024E, for example,

Table 1
Details of samples collected across the BMGP.

Sample name	Latitude (S)	Longitude (W)	Elevation (m)	Field description
FV-R−003B	16° 09' 20.87"	39° 55' 11.00'	189	Saprolitic graphite-rich paragneiss
FV-R-003C	17° 09' 20.87"	39° 55' 11.00'	189	Saprolitic graphite-rich paragneiss
FV-R−003D	18° 09' 20.87"	39° 55' 11.00'	189	Saprolitic graphite-rich paragneiss
FV-R−005B	16° 05' 38.42"	40° 01' 57.09"	147	Intensely folded graphite-rich paragneiss
FV-R−024D	15° 46' 19.52"	41° 01' 47.13"	728	Biotite-graphite schist
FV-R−024E	15° 46' 19.52"	41° 01' 47.13"	728	Mylonitic graphite-rich schist
FV-R−059B	15° 54' 58.66"	40° 54' 51.11"	579	Migmatitic graphite-rich paragneiss
FV-R-007C	15° 52' 17.94"	40° 21' 45.08"	528	Graphite paragneiss
FV-R−007D	15° 52' 17.94"	40° 21' 45.08"	528	Graphite paragneiss
FV-R−007E	15° 52' 17.94"	40° 21' 45.08"	528	Garnet-cordierite-graphite paragneiss
EM-R−060	15° 50' 12.33"	40° 33' 13.21"	292	Graphite schist
EM-R−062B	15° 49' 31.49"	40° 32' 31.80"	308	Graphite schist
FV-R−209A	15° 48' 46.08"	40° 19' 23.80"	259	Graphite gneiss
FV-R−212	15° 52' 44.23"	40° 18' 01.75"	260	Graphite gneiss

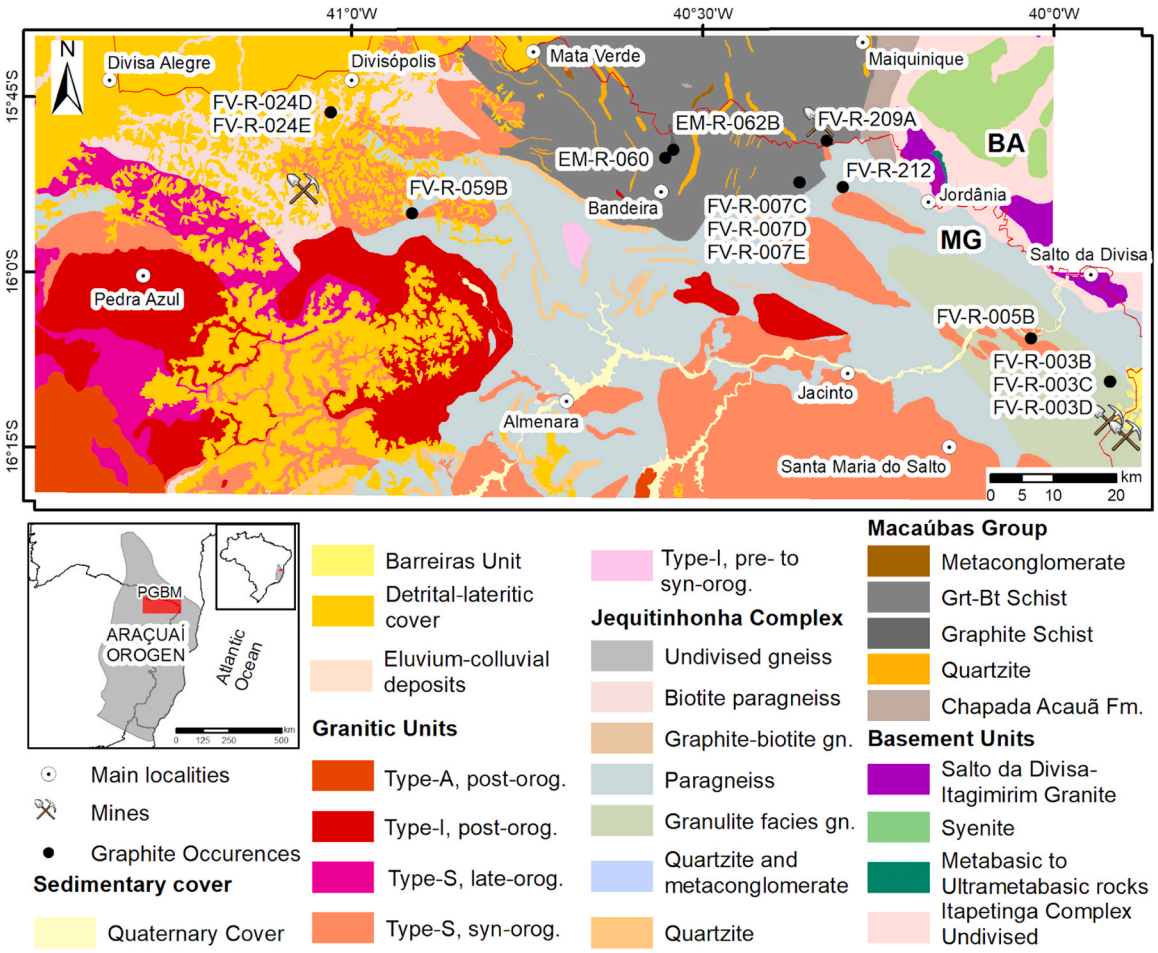


Fig. 1. Geological map of the field area with sample locations provided. Map prepared by F T Vilela using SGB data and simplified from Silva et al. (2020). © SGB 2025.

where flake graphite is present, muscovite, biotite, a Ti-rich micaceous phase, kaolinite, chlorite, K-feldspar, and quartz are all present within or proximal to graphite (Fig. 4). These gangue minerals in graphite tend to range from submicron to hundreds of microns in length and range from angular grains, like quartz, to more elongate, like muscovite and kaolinite (Fig. 4).

4.2. In-lens results

The in-lens detector was used to better understand submicron-scale gangue minerals associated with flake graphite in samples FV-R−003, FV-R−005B, and FV-R−024E. At the submicron scale and based on analysis of these samples, it is likely that quartz and K-feldspar are the dominant subangular gangue minerals. Jarosite appears less frequently and is more subrounded in morphology, whilst kaolinite appears homogenous and intergrown with graphite mineralization. In-lens also afforded the opportunity to view the layered structure of graphite flakes in their raw form as illustrated by Kim et al. (2003).

The following section provides selected examples from in-lens analyses.

In sample FV-R−003, subangular, microtextured quartz grains appear to have crystallized adjacent to or within fractures between expanded or stacked graphite flake clusters (Fig. 4c, d). These quartz grains can be described as somewhere between type 1 (simple substance between graphite clusters) or as type 2 (small, microtextured substance between graphite clusters) (Kim et al., 2003).

In sample FV-R−005B, similar subangular, microtextured quartz and kaolinite is observed in a fractured area between stacked graphite flake clusters (Fig. 5). Again, these impurities could be described as somewhere between type 1 and 2. In the same sample, subrounded jarosite is observed in contact with flakes of graphite and could be described as a type 1 impurity (Fig. 7).

In sample FV-R−024E, kaolinite is observed as smooth, homogenous material intergrown with the adjacent graphite (Fig. 8). The kaolinite may be described as a type 4 impurity (a flat impurity sandwiched between the stacks within a cluster) (Kim et al., 2003).

The morphology of graphite flakes has been revealed to be layered and composed of clusters of stacks with a variety of gangue mineral impurities, or intercalants, as described by Kim et al. (2003) (Fig. 9).

5. Discussion

5.1. Considerations for graphite formation conditions

The mineral assemblage associated with flake graphite provides insights into the metamorphic conditions that governed graphite formation. BSE-EDX analyses reveal kaolinite as the dominant gangue mineral, frequently found within graphite cleavages or adjacent asperities, followed by quartz in lesser abundance. A broader suite of accessory minerals including smectite-group clays, tourmaline, sillimanite, K-feldspar, albite, calcic plagioclase, zircon, xenotime, jarosite, Fe-oxides, Ti-oxides, Fe-sulfides, and rutile also occurs sporadically within or near graphite flakes and can inform metamorphic and fluid interaction histories. The following discussion will highlight key indicators of metamorphic and fluid interaction history for this sample set and will compare our findings to existing literature.

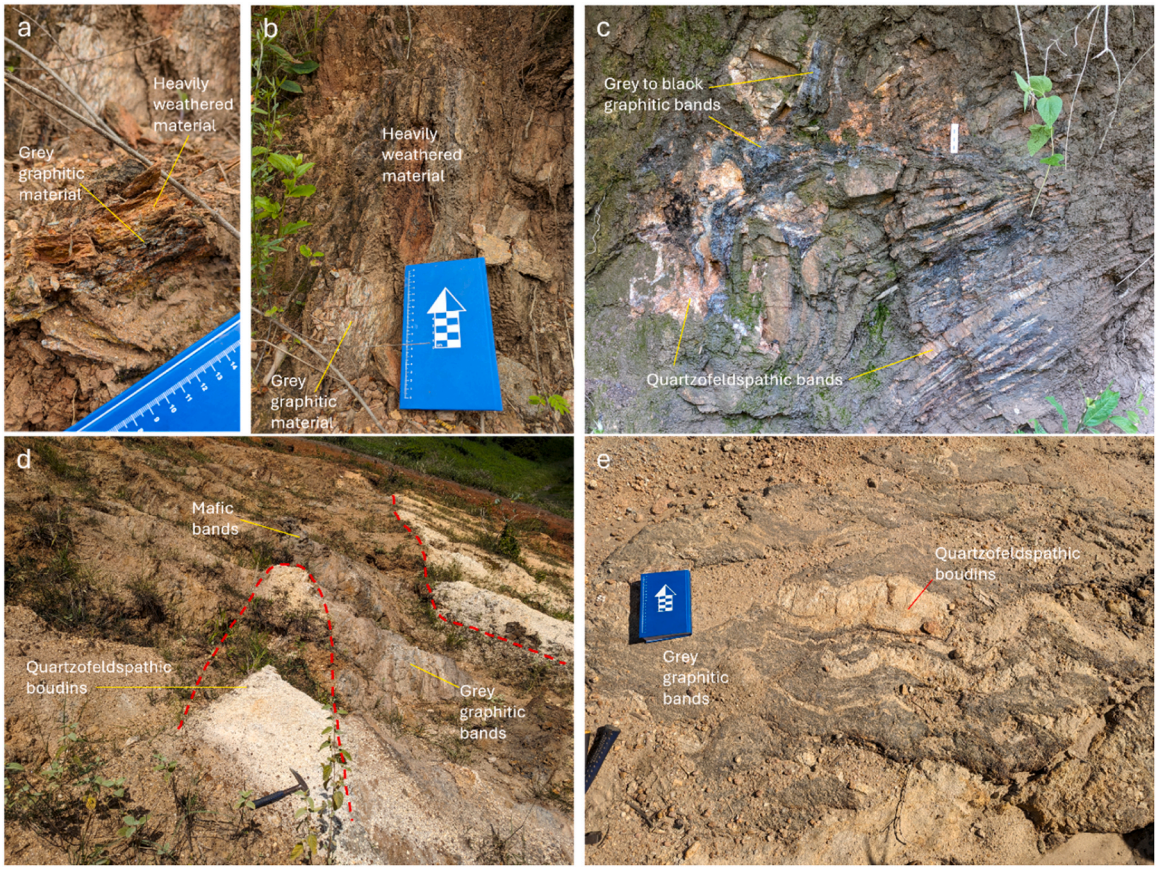


Fig. 2. Selection of field photographs highlighting macro/outcrop-scale metamorphic textures. (a) and (b) Thin slivers of heavily weathered mylonitic graphite-rich schistose material (FV-R−024D and E). (c) Intensely folded, graphite-rich paragneiss and leucosomal quartzofeldspathic bands (FVR−059B). (d) An example of the macroscopic-scale boudinage of leucosomal bands adjacent to graphitic and mafic material (FV-R−003B, C, D). (e) Road exposure of boudinaged quartzofeldspathic bands amongst grey graphite-rich bands (FV-R−005B).

The presence of sillimanite, muscovite, biotite, and K-feldspar indicates medium- to high-grade metamorphic conditions, typically within the amphibolite facies where temperatures exceed 500°C (Spear, 1993; Pedrosa-Soares and Wiedemann-Leonardos, 2000; Belém, 2006; Bucher and Grapes, 2011). The coexistence of muscovite and sillimanite may suggest transitional conditions or incomplete reaction progress, as muscovite generally breaks down at temperatures above 650°C in the presence of quartz to form sillimanite and K-feldspar (Powell and Holland, 2008). Sillimanite is a reliable indicator of high-temperature metamorphism, while muscovite and biotite reflect a pelitic protolith.

In sillimanite-grade rocks, the coexistence of tourmaline with high-temperature minerals like sillimanite and flake graphite implies metamorphic conditions within the amphibolite facies, typically exceeding 500°C (Henry and Dutrow, 1996; Dutrow and Henry, 2000; Bucher and Grapes, 2011). Tourmaline's stability across a wide pressure and temperature range allows it to persist through prograde and retrograde metamorphism, making it an indicator of fluid activity and metamorphic grade. Its presence also supports a sedimentary origin for the protolith, as boron is often concentrated in marine sediments rich in organic matter. This is consistent with the interpretation of graphite as metamorphosed carbon derived from Precambrian, organic-rich layers (Pedrosa-Soares and Wiedemann-Leonardos, 2000; Pacheco et al., 2021).

In contrast, kaolinite, smectite, and chlorite are generally stable under low-grade metamorphic or diagenetic conditions, implying either retrograde alteration or incomplete metamorphism in localized domains (Inoue et al., 1987; Jambor et al., 2000; Tetiker et al., 2015). Moreover, the jarosite within sillimanite-graphite gneiss is notable as jarosite typically forms under low-temperature, oxidizing, and acidic conditions (Cruells and Roca, 2022). Its presence suggests post-peak metamorphic alteration, likely driven by fluid infiltration during uplift or surface exposure. Jarosite commonly precipitates from the oxidation of iron sulfides such as pyrite or pyrrhotite in the presence of sulfate-rich, acidic fluids (Cruells and Roca, 2022). This implies that the sample set experienced supergene weathering or hydrothermal overprinting after the main metamorphic event. Furthermore, jarosite's stability is limited to temperatures below around 150°C, reinforcing its interpretation as a secondary phase formed during retrograde alteration or surface weathering (Papike et al., 2006). Jarosite's presence in sillimanite-graphite gneiss therefore marks a significant shift in redox conditions and fluid chemistry, pointing to an open-system metamorphic evolution.

The interpretation presented aligns closely with previous work on the Jequitinhonha Complex in the BMGP, which hosts Brazil's largest flake graphite reserves. The Jequitinhonha Complex is composed of aluminium-rich kinzigitic paragneisses (sillimanite cordierite-garnet-biotite gneiss with traces of graphite), interlayered with graphite gneisses, quartzites, and calc-silicate lenses, and was metamorphosed at the amphibolite–granulite facies transition between 550 and 570 Ma (Gonçalves-Dias et al., 2016; Pacheco et al., 2021). The sedimentary protoliths of the Jequitinhonha Complex are interpreted as part of a Cryogenian passive margin sequence within the precursor basin of the Araçuaí Orogen (Gonçalves-Dias et al., 2011; Pedrosa-Soares et al., 2011).

In contrast, the Macaúbas Group, also within the BMGP, represents a lower metamorphic grade, with graphite hosted in greenschist-facies schists. Graphite in these rocks is typically smaller in size and less crystalline, reflecting the lower temperature conditions of metamorphism. Belém (2006) reports graphite flake sizes in the Macaúbas

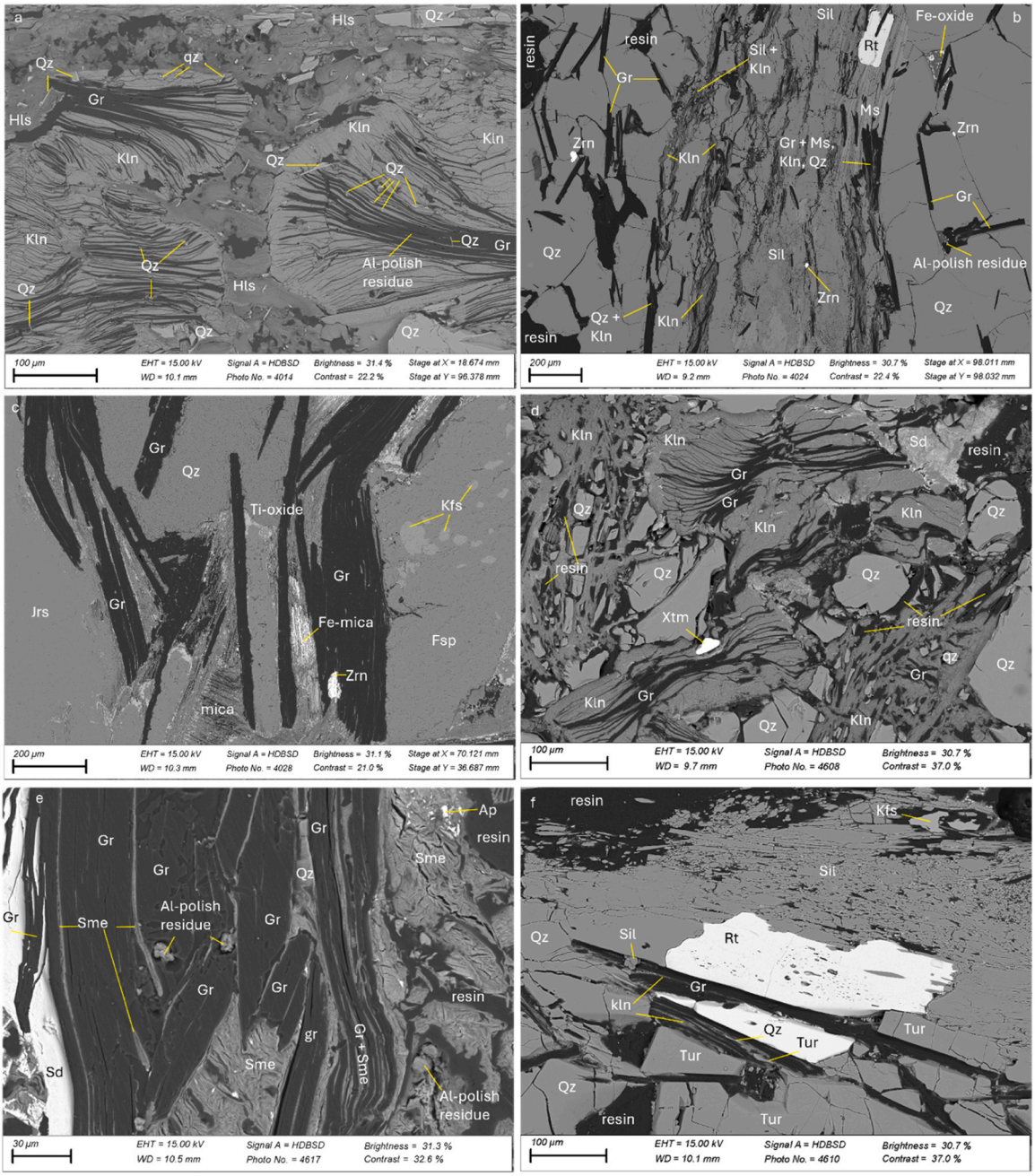


Fig. 3. (a) Backscatter electron (BSE) image of FV-R−059B showing splayed opaque flake graphite hosted by kaolinite in a halloysite matrix with subangular quartz grains across the sample. Quartz and kaolinite can be seen between the graphite flake cleavage in multiple locations. (b) BSE image of EM-R−060 showing opaque flake graphite primarily hosted by quartz and by a sillimanite, muscovite, kaolinite, and quartz matrix. Quartz and kaolinite are the primary minerals between graphite flake cleavage, though minor sillimanite and muscovite also appear as intercalation in places. (c) BSE image of FV-R−005B showing opaque flake graphite hosted in a heavily altered mica with Ti-rich grain rims. This altered mica can be found between graphite cleavage as can jarosite and quartz. (d) BSE image of FV-R−209A showing opaque splayed flake graphite primarily hosted by kaolinite. Kaolinite and quartz can be found between graphite cleavages. (e) BSE image of FV-R−003 showing opaque flake graphite hosted by a smectite-group clay phase. This smectitic clay is prevalent between graphite cleavage. (f) BSE image of FV-R−212 showing opaque flake graphite in a quartz, tourmaline, sillimanite, and rutile matrix. These minerals, and kaolinite, can all be found between graphite cleavages. Mineral abbreviations from Whitney and Evans (2010).

Group ranging from 0.10 to 0.30 mm, whereas flakes in the Jequitinhonha Complex range from 0.30 mm to 1 cm, classified as flake to super jumbo. The graphite flakes observed in the current study fall within the flake to jumbo size fraction (106–500 μm), consistent with the Jequitinhonha Complex and indicative of similar metamorphic conditions previously discussed.

5.2. *Implications for depositional environment of graphite source material*

The BMGP hosts vast economic deposits of flake graphite, considered amongst the largest graphite ore provinces globally, with estimates suggesting over a billion tons of raw graphite reserves (Belém, 2006, 2018; Pacheco et al., 2021). The depositional environment of the Jequitinhonha paleobasin has been interpreted as being predominantly quiet-water and marine in nature (Pacheco et al., 2021). Evidence is

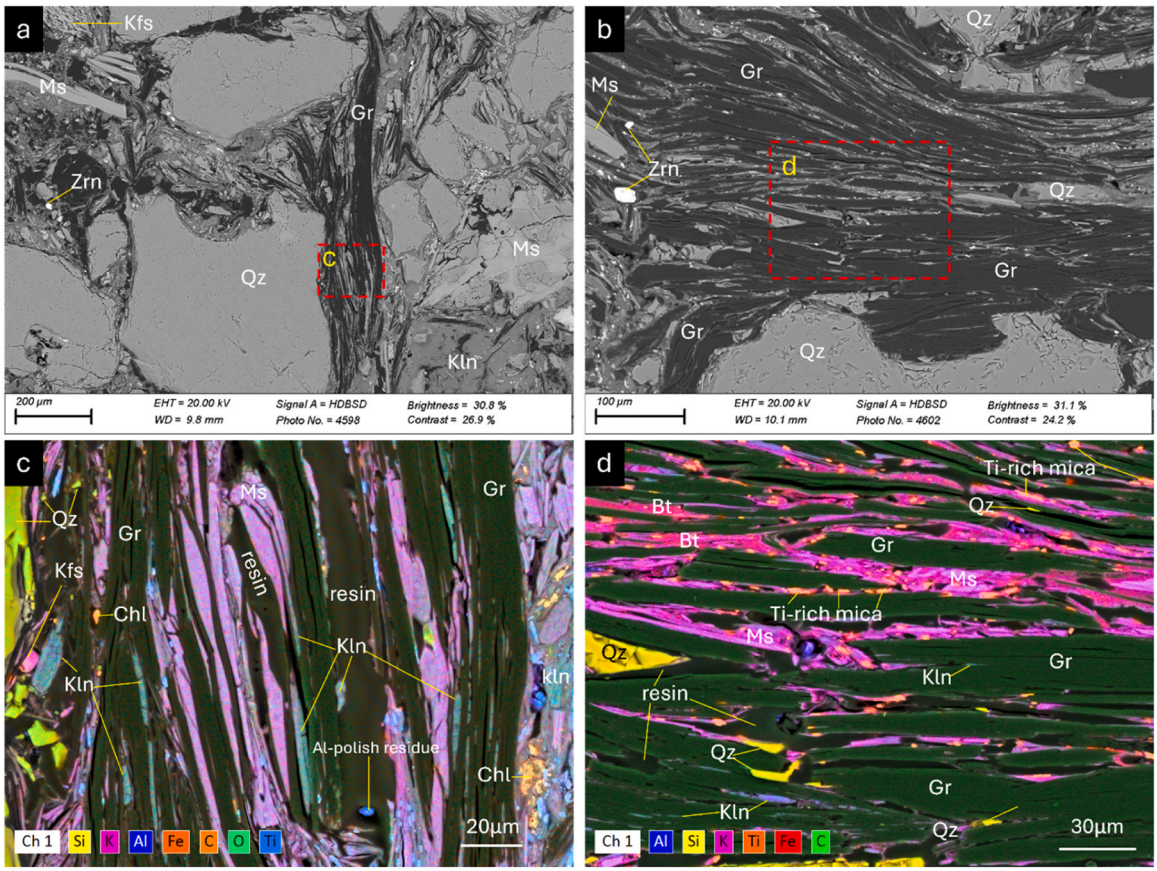


Fig. 4. BSE (a; b) and EDS (c; d) images of sample FV-R−024E. Red dashed box refers to the areas where images c and d were taken from in images a and b, respectively. (a and c) opaque flake graphite appears to be up to 20 µm wide and contains grains of quartz, K-feldspar, chlorite, muscovite, and kaolinite. (b and d) opaque flake graphite appears to be upwards of 30 µm wide and contains grains of muscovite, biotite, a Ti-rich mica phase, quartz, and kaolinite within cleavages and interspersed between flakes. Mineral abbreviations from Whitney and Evans (2010).

provided by the widespread presence of aluminium-rich paragneiss, which originated from clay-rich pelitic sediments. These sediments were likely laid down under low-oxygen (anoxic) conditions, key conditions for the preservation of organic material that would later transform into graphite during metamorphism. The regional lithological assemblage, comprising sillimanite-graphite gneiss (metamorphosed carbonaceous mud), quartzite, kinzigitic gneiss (metapelite), and calc-silicate rocks derived from marls, shows no signs of volcanic influence. This supports a purely sedimentary origin for the carbon-rich layers, reinforcing the idea that the graphite formed from organic matter deposited in a stable, low-energy marine setting (Pedrosa-Soares and Wiedemann-Leonardos, 2000).

Overall, the mineralogical evidence presented in this study supports a model in which graphite formed under amphibolite-facies conditions, followed by retrograde overprinting or localized low-grade alteration. These findings align with broader interpretations of the Jequitinhonha Complex, where sedimentary, carbon-rich layers underwent high-grade metamorphism, yet preserved a record of Precambrian organic matter in graphite-rich gneisses (Pedrosa-Soares and Wiedemann-Leonardos, 2000; Belém, 2006, 2018; Pacheco et al., 2021).

5.3. Significance of in-lens results

The in-lens analysis of graphite-bearing samples FV-R−003B, FV-R−005B, and FV-R−024E shows quartz, K-feldspar, kaolinite, and jarosite as the main phases associated with flake graphite at the submicron scale. These minerals exhibit distinct morphologies and spatial relationships with graphite flakes, which align closely with the impurity classification system proposed in the study on gangue mineral inclusion and mechanical separation from expanded graphite by Kim et al. (2003).

The four impurity types, based on their position and morphology relative to graphite flakes, are as follows:

- type 1: simple substances between graphite clusters
- type 2: small microtextured substances between clusters
- type 3: impurities embedded within flakes
- type 4: flat impurities sandwiched between graphite stacks

In samples FV-R−003B and FV-R−005B, subangular quartz and K-feldspar grains are observed within fractures between graphite clusters, corresponding to type 1 and type 2 impurities. These findings suggest that these minerals were either mechanically entrapped during graphite stacking or introduced during late-stage deformation. Jarosite, observed in FV-R−005B as subrounded and in contact with graphite flakes, also fits the type 1 classification. However, its formation likely reflects post-metamorphic oxidation of sulfides under acidic conditions, indicating supergene alteration, a process not addressed in the mechanical separation framework of Kim et al. (2003). In contrast, FV-R−024E displays kaolinite as a smooth, homogenous phase intergrown with graphite, consistent with type 4 impurities. This morphology suggests early diagenetic incorporation or retrograde alteration, differing from the mechanically entrapped clays described by Kim et al. (2003).

Our study provides the mineralogy, petrology, and metamorphic history that is often lacking in mineral processing frameworks like Kim et al. (2003). Submicron-scale information on these natural mineral impurities that formed through geological processes may provide greater insight into applicable practical workflows for mineral processing of natural materials and may provide insight into

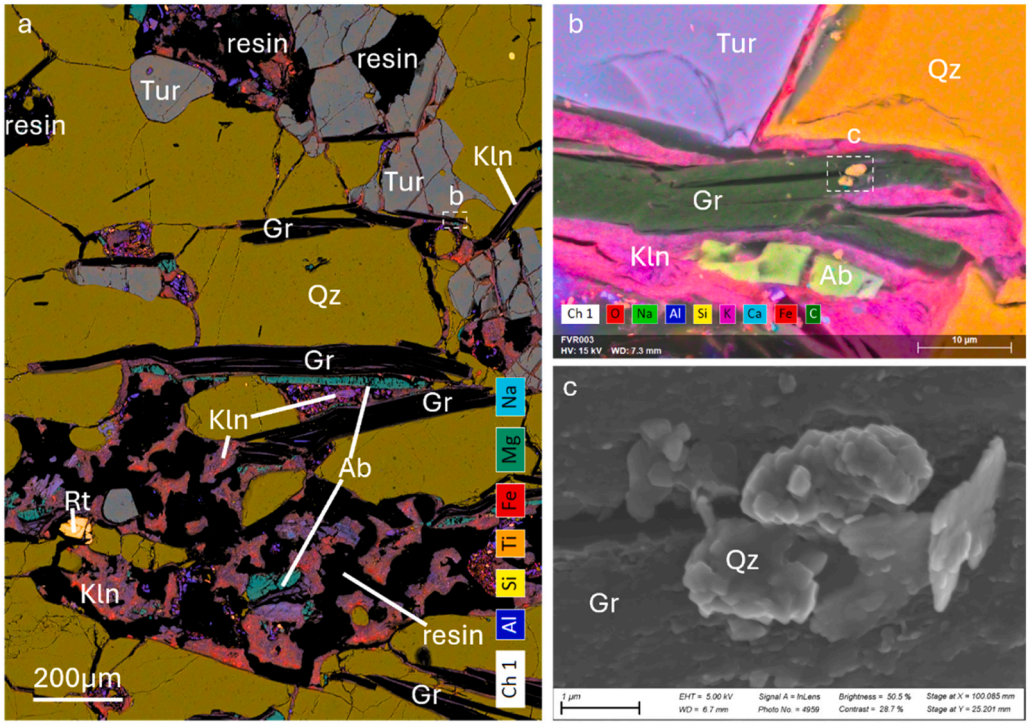


Fig. 5. Sample FV-R−003B. (a) BSE-EDX image with mineralogy shown. (b) BSE-EDX image of box b from image (a) highlighting the quartz gangue minerals within graphite mineralization. (c) In-lens image of quartz grains in box c from image (b). Quartz grains here appear to be subangular, simple substances held between graphite clusters and can be attributed as type 1 impurities based on Kim et al. (2003). Mineral abbreviations from Whitney and Evans (2010).

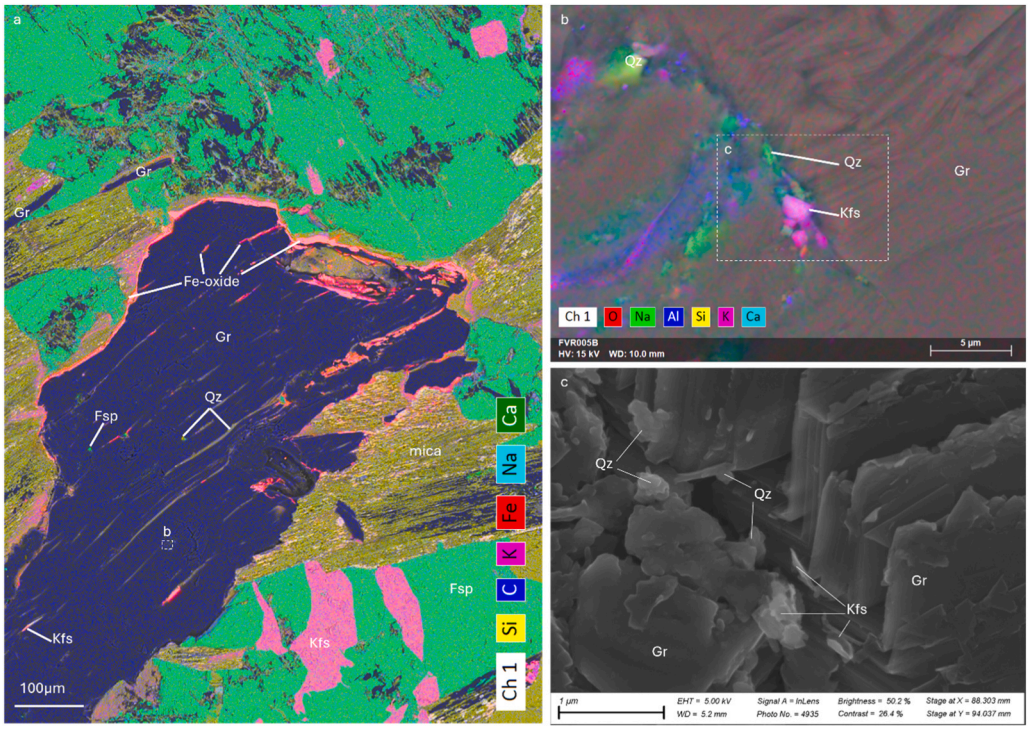


Fig. 6. Sample FV-R−005B. (a) BSE-EDX image with mineralogy shown. (b) BSE-EDX image of box b from image (a) highlighting the quartz and K-feldspar gangue minerals within graphite mineralization. (c) In-lens image of quartz and K-feldspar grains in box c from image (b). Quartz and K-feldspar grains here appear to be subangular, simple substances held between graphite clusters and can be attributed as type 1 to type 2 impurities based on Kim et al. (2003). Mineral abbreviations from Whitney and Evans (2010).

post-processing environmental risks and mitigations. The following section briefly identifies such risks and mitigations.

Graphite flakes consist of stacked graphene layers held together by weak van der Waals forces, making them prone to delamination and fragmentation during aggressive comminution (Wang et al., 2024). The in-lens observations in this study show that flakes often form clustered

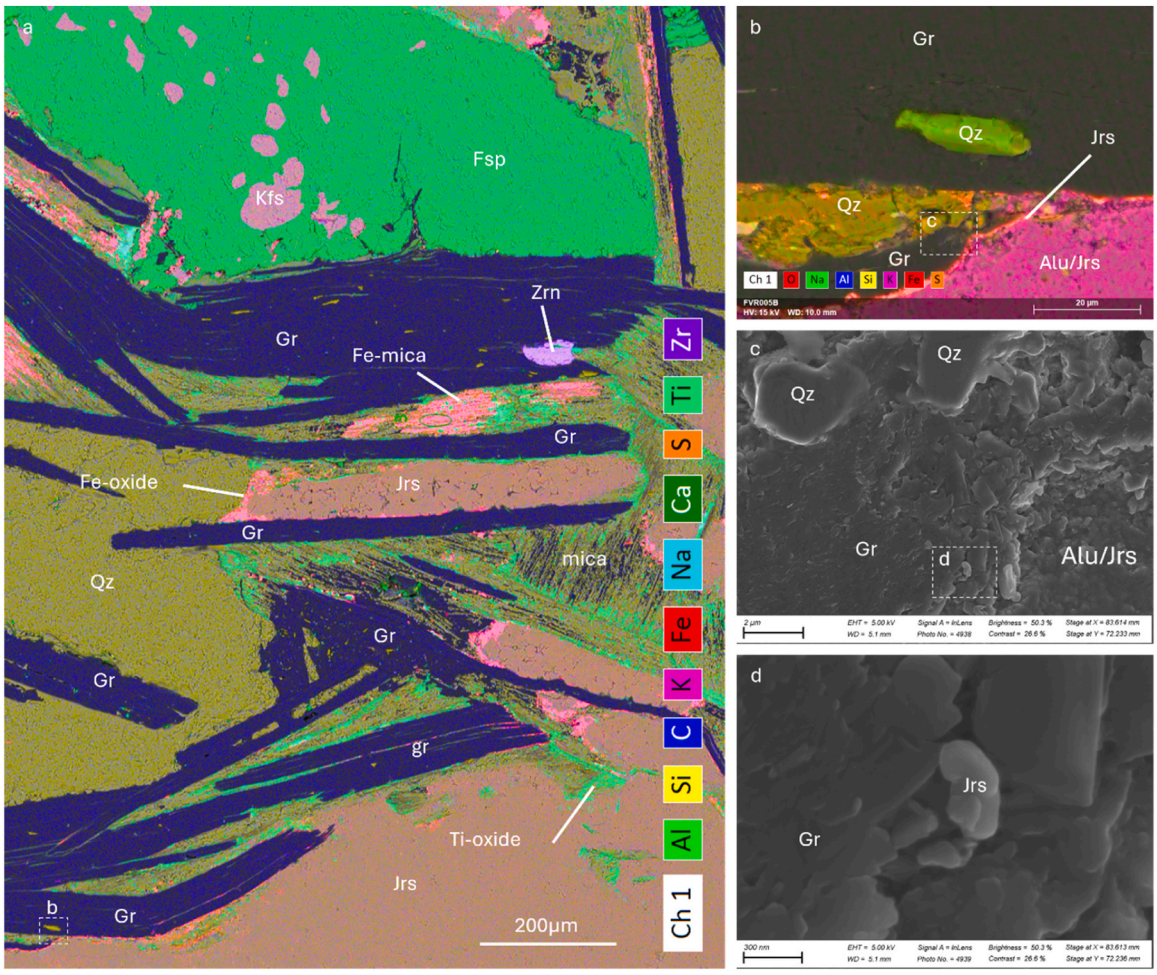


Fig. 7. Sample FV-R−005B. (a) BSE-EDX image with mineralogy shown. (b) BSE-EDX image of box b from image (a) highlighting the gangue minerals within or adjacent to graphite mineralization. (c) In-lens image of subangular quartz and subangular to subrounded jarosite/alunite grains adjacent to graphite. (d) In-lens image of box d from image (c) highlighting the morphology of a jarosite grain, which can be attributed as a type 1 impurity based on Kim et al. (2003). Mineral abbreviations from Whitney and Evans (2010).

stacks with interstitial gangue minerals, which, if not carefully liberated, can exacerbate flake damage during grinding and separation (Wang et al., 2024). Quartz and K-feldspar impurities may require controlled milling, low-energy attrition milling, or pneumatic separation to avoid excess graphite fragmentation (Chehreh Chelgani et al., 2016). The presence of kaolinite may require chemical or flotation separation for effective liberation (Zanin et al., 2019).

To mitigate this, pre-screening and classification techniques should be employed early in the beneficiation workflow to isolate coarse flakes before they are exposed to high-energy milling. This allows for size-specific handling and reduces unnecessary exposure to mechanical forces. Pneumatic separation and low-energy attrition methods have shown promise in preserving flake integrity by minimizing interparticle collisions and shear stress (Liu and Ma, 2024). These approaches are particularly effective for high-grade, larger flake graphite ores where flake size retention is critical.

The implications of the findings revealed by this study are significant for high-value applications. As Jara et al. (2019) emphasizes, flake size and morphology directly influence graphite's thermal conductivity, electrochemical performance, and mechanical strength. In lithium-ion batteries, for example, larger flakes offer higher conductivity and lower irreversible capacity loss, and in thermal management systems, intact flakes enhance heat dissipation due to their anisotropic conductivity (Li and Zhou, 2012; Zhao et al., 2022).

The presence of jarosite may indicate the need for pH control in flotation circuits to avoid damage to hardware since it can have acid-generating potential and disrupt flotation circuits by lowering pH (Chen et al., 2025). Jarosite can also cause issues around tailings handling, slurry transportation, and waste stabilization in large-scale operations. Thus, mine sites may need to apply appropriate environmental mitigation measures around any tailing ponds and run-off areas where jarosite is or could be present (Cruells and Roca, 2022; Akhtar and Kulhary, 2025).

Understanding the spatial distribution of gangue minerals and the structural sensitivity of graphite can enable processors to design workflows that balance liberation efficiency with product quality, ultimately enhancing the performance of graphite in advanced technological applications. We suggest that by integrating microtextural insights from nanoscale SEM imaging with targeted industrial processing strategies, this study supports a beneficiation model that prioritizes flake preservation and therefore value-addition for producers of Brazilian flake graphite ore materials.

6. Conclusion

This study demonstrates that flake graphite in the Bahia–Minas Graphite Province is consistently associated with a limited set of gangue minerals, dominated by kaolinite and quartz, with subordinate feldspars and minor secondary phases such as jarosite. These minerals occur both as mechanically entrapped particles and as intergrown phases within

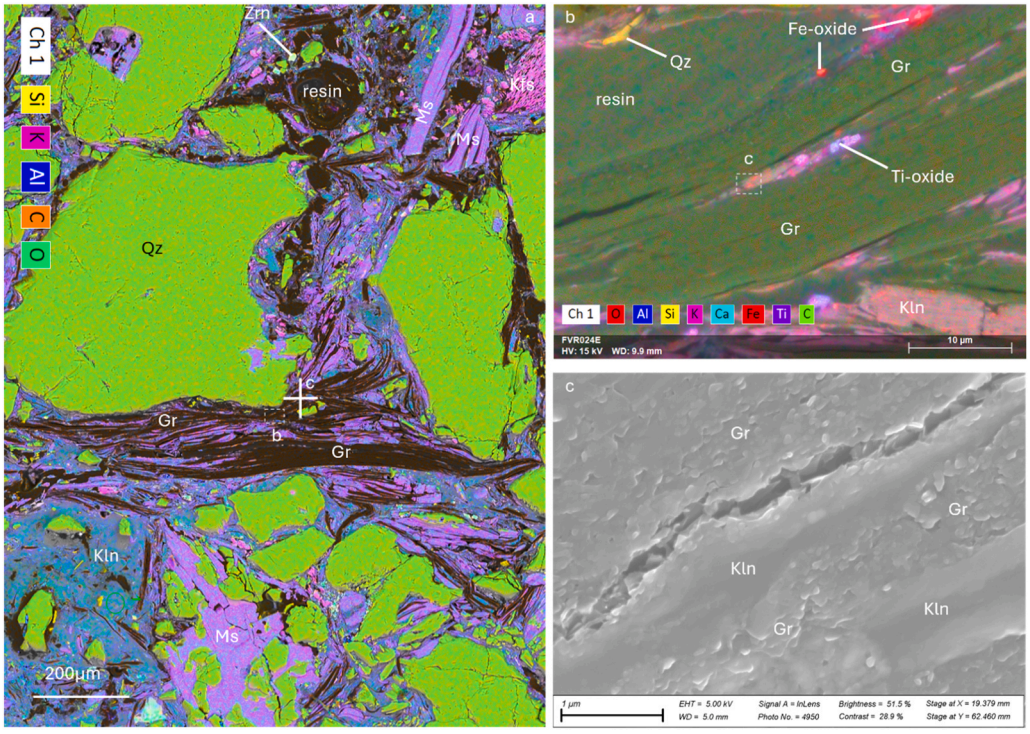


Fig. 8. Sample FV-R−024E. (a) BSE-EDX image with mineralogy shown. (b) BSE-EDX image of box b from image (a) highlighting the quartz, kaolinite, and Ti- and Fe-oxides within and adjacent to graphite. (c) In-lens image of kaolinite grains highlighted using the + sign on image (a) and box b in image (c). Kaolinite is observed as smooth, homogenous material intergrown with the adjacent graphite and can be attributed as type 4 impurities based on Kim et al. (2003). Mineral abbreviations from Whitney and Evans (2010).

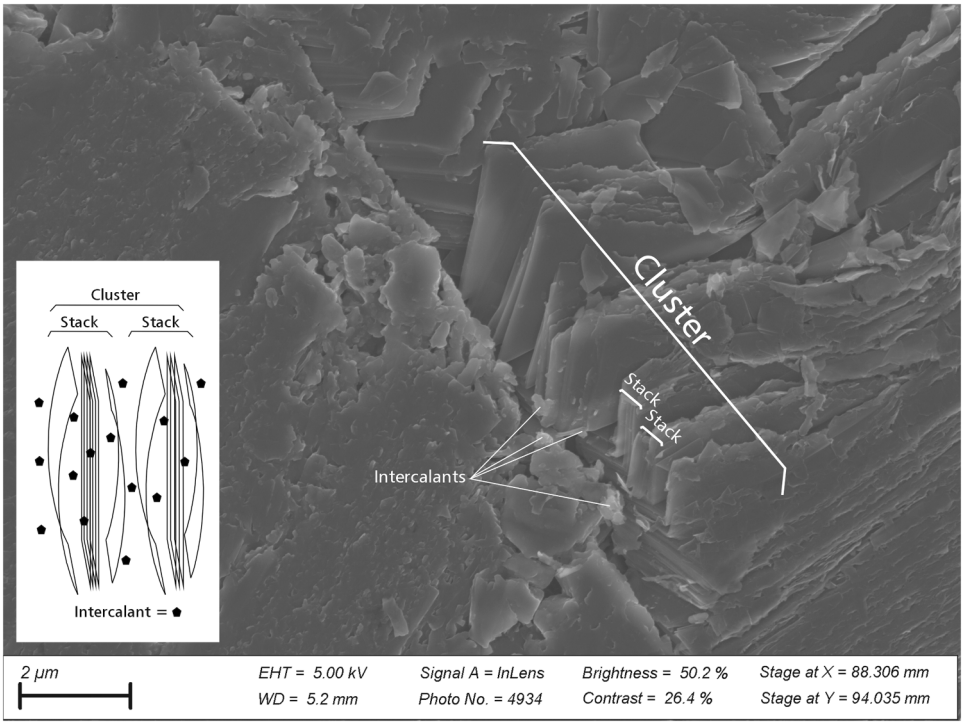


Fig. 9. Inset image in bottom left is an illustration showing typical formation of flake graphite in raw material adapted from Kim et al. (2003). Main image is a representative example of this in nature using sample FV-R-005B.

graphite cleavages, reflecting distinct modes of incorporation.

Microtextural evidence shows that quartz and feldspar typically form discrete, weakly bound inclusions, whereas kaolinite commonly occurs as intergrown material within graphite stacks. This distinction is critical, as it directly influences the ease of liberation and the susceptibility of graphite flakes to damage during processing.

The combined SEM and in-lens observations confirm that graphite occurs as stacked flake aggregates hosting interstitial gangue minerals at the micro- to submicron scale. This architecture highlights the structural sensitivity of graphite and explains the strong dependence of product quality on controlled liberation.

These findings provide a mineralogical basis for predicting beneficiation behaviour: mechanically trapped silicates are more amenable to physical separation, while intergrown clays require more selective or chemical approaches. Recognition of impurity type and distribution therefore, enables more effective processing strategies that prioritise flake preservation.

Overall, this study establishes a direct link between gangue mineral morphology, graphite texture, and processing response, therefore offering a framework for improving recovery, maintaining flake integrity, and enhancing graphite quality in the BMGP and comparable deposits globally.

6.1. Future work

To advance graphite beneficiation and fully integrate mineralogical insights into processing workflows, future research must focus on refining the characterization of gangue minerals and understanding their behaviour during separation. While in-lens has revealed key impurities such as quartz, K-feldspar, kaolinite, and jarosite, further work using Raman spectroscopy, XRD, and microprobe analysis is needed to resolve phase chemistry and trace element associations, particularly for clays and secondary sulfates. Quantitative liberation studies should assess graphite flake damage under varying milling regimes, using image analysis and automated mineralogy tools to model gangue-host relationships and optimize comminution strategies.

Flotation behaviour of fluid-sensitive minerals like kaolinite and jarosite also warrants investigation, especially under controlled pH and reagent conditions. Understanding surface chemistry and reagent interactions will improve selectivity and reduce flake attrition. Additionally, jarosite's acid-generating potential and metal content necessitate environmental risk assessments, including leach testing and tailings stability modelling.

Finally, integrating mineralogical data into predictive processing models could enable dynamic adjustment of beneficiation parameters based on ore variability. Together, these research directions could bridge the gap between geological complexity and processing efficiency, ensuring graphite flake preservation and enhancing product performance in high-value applications while potentially mitigating environmental risks.

CRediT authorship contribution statement

David Currie: Writing – review & editing, Writing – original draft, Validation, Software, Resources, Project administration, Methodology, Investigation, Formal analysis, Data curation, Conceptualization. **Vilela Francisco:** Writing – review & editing, Writing – original draft, Visualization, Validation, Resources, Methodology, Investigation, Formal analysis, Data curation, Conceptualization. **Matos Debora:** Writing – review & editing, Writing – original draft, Visualization, Validation, Resources, Investigation, Data curation. **Araujo Joanna:** Writing – review & editing, Writing – original draft, Validation, Resources, Project administration, Investigation, Data curation.

Funding

This work was supported by the British Geological Survey via NERC national capability E9147S and E7891.

Declaration of Competing Interest

The authors declare that they have no known competing financial interests or personal relationships that could have appeared to influence the work reported in this paper.

Acknowledgements

The authors would like to thank:

- Dr Kathryn Goodenough for establishing this working relationship between BGS and SGB.
- Dr Guilherme Ferreira da Silva and all involved staff for hosting BGS staff at the Belo Horizonte office.
- Dr Jeremy Rushton for technical assistance with scanning electron microscopy at BGS, Keyworth.
- landowners across the BMGP field area for their cooperation and friendliness during our fieldwork.
- Clive Mitchell for internally reviewing the initial manuscript.
- The two anonymous reviewers for their constructive feedback and the valuable time they dedicated to evaluating our manuscript. Their insights have significantly improved the quality of our work.

This paper is published by permission of the Director of the British Geological Survey.

Data availability

Data will be made available on request.

References

Akhtar, V., Kulhary, D., 2025. Physico-chemical characterization and environmental implications of jarosite waste. Asian J. Chem. 37 (8).
Belém, J., 2006. Caracterização mineralógica, física e termobarométrica de minérios de grafita da Província Grafítica Bahia-Minas. Instituto de Geociências. Universidade Federal de Minas Gerais, Belo Horizonte.
Belém, J., 2018. Recursos Minerais de Minas Gerais – Grafita. CODEMG (Companhia de Desenvolvimento Econômico de Minas Gerais), Belo Horizonte.
Bucher, K., Grapes, R.H., 2011. Petrogenesis of metamorphic rocks, 8th ed. Springer, Berlin.
Chehreh Chelgani, S., Rudolph, M., Kratzsch, R., Sandmann, D., Gutzmer, J., 2016. A review of graphite beneficiation techniques. Mineral. Process. Extr. Metall. Rev. 37, 58–68.
Chen, M., Wang, R., Fan, W., Wang, J., Zeng, X., Han, Y., Liang, Q., Huang, R., Zhou, S., Shu, J., 2025. Advances on jarosite residue detoxification and reutilization: a review. Environ. Sci. Pollut. Res. 32, 3571–3592.
Cruells, M., Roca, A., 2022. Jarosites: structure, formation, leaching, environmental, and applications. Metals 12 (5), 802.
Currie, D., Araujo, J.C.S., Vilela, F.R., Matos, D.R., 2024. Graphite reconnaissance, Minas Gerais – Bahia region, Brazil, March 2024. Br. Geol. Surv. Open. Report. 26–28. OR/25/051,.
Dutrow, B.L., Henry, D.J., 2000. Tourmaline as a recorder of metamorphic conditions. Rev. Mineral. Geochem. 33 (1), 407–432.
Farquhar, J., Hauri, E., Wang, J., 1999. New insights into carbon fluid chemistry and graphite precipitation: SIMS analysis of granulite facies graphite from Ponmudi, South India. Earth Planet. Sci. Lett. 171, 607–621.
Gonçalves-Dias, T., Caxito, F., Pedrosa-Soares, A.C., Stevenson, R., Dussin, I., Da Silva, L., Alkmim, F., Pimentel, M., 2016. Age, provenance and tectonic setting of the high-grade Jequitinhonha Complex, Araçuaí Orogen, eastern Brazil. Braz. J. Geol. 46, 199–219.
Gonçalves-Dias, T., Pedrosa-Soares, A.C., Dussin, I.A., de Alkmim, F.F., Caxito, F.A., da Silva, L.C., Noce, C.M., 2011. Idade máxima de sedimentação e proveniência do Complexo Jequitinhonha na área-tipo (Orógeno Araçuaí): primeiros dados U-Pb (LA-ICP-MS) de grãos detríticos de zircão. Geonomos.
Henry, D.J., Dutrow, B.L., 1996. Metamorphic tourmaline and its petrologic applications. Geol. Soc. Am. Abstr. Prog. 28 (7) p.A-504.
Hund, K., Porta, D., Fabregas, T., Laing, T., Drexhage, J., 2023. Minerals for climate action: The mineral intensity of the clean energy transition.
Idoine, N.E., Raycraft, E.R., Evans, E.J., Mills, A.J., Shaw, I.R., Watkins, I., Albornoz-Parra, L., Everett, P., Hobbs, S.F., Shaw, R.A., 2026. World mineral production 2020-24. Nottingham, UK, British Geological Survey, 102pp. (World Mineral Production).
IEA, 2024. Global Critical Minerals Outlook 2024. International Energy Agency, Paris.
Inoue, A., Meunier, A., Patrier-Mas, P., Rigault, C., Beaufort, D., Vieillard, P., 1987. Illite-smectite mixed-layer minerals in diagenetic and low-grade metamorphic rocks: a review. Clays Clay Miner. 35 (5), 289–302.
Jambor, J.L., Nordstrom, D.K., Alpers, C.N., 2000. Sulphate minerals: crystallography, geochemistry, and environmental significance. Rev. Mineral. Geochem. 40, 303–350.

Jara, A.D., Betemariam, A., Woldetinsae, G., Kim, J.Y., 2019. Purification, application and current market trend of natural graphite: a review. Int. J. Min. Sci. Technol. 29, 671–689.
Jara, A.D., Woldetinsae, G., Betemariam, A., Kim, J.Y., 2020. Mineralogical and petrographic analysis on the flake graphite ore from Saba Boru area in Ethiopia. Int. J. Min. Sci. Technol. 30, 715–721.
Kim, B.G., Choi, S.K., Park, C.L., Chung, H.S., Jeon, H.S., 2003. Inclusion of gangue mineral and its mechanical separation from expanded graphite. Part. Sci. Technol. 21, 341–351.
Li, Z., Larkin, T., Urbas, A., Li, Y., Ruan, G., Kittrell, C., Zhao, Y., Yan, K., Zhu, Y., Tour, J. M., Ruoff, R.S., 2007. X-ray diffraction patterns of graphite and turbostratic carbon. Carbon 45, 1686–1695.
Li, K., Zhang, Y., Liu, Y., Wang, L., Wang, H., Li, Y., Li, Y., Huang, Y., 2021. Classification and carbon structural transformation from anthracite to natural coaly graphite by XRD, Raman spectroscopy, and HRTEM. Spectrochim. Acta Part. A Mol. Biomol. Spectrosc. 249, 119286.
Li, H., Zhou, H., 2012. Enhancing the performances of Li-ion batteries by carbon-coating: present and future. Chem. Commun. 48 (9), 1201–1217.
Liu, H., Ma, F., 2024. Study on the effect of high-pressure grinding rolls on the liberation of fine flake graphite. China Min. Mag. 33 (4), 227–232.
Luque, F.J., Huizenga, J.M., Crespo-Feo, E., Wada, H., Ortega, L., Barrenechea, J.F., 2014. Vein graphite deposits: geological settings, origin, and economic significance. Miner. Depos. 49 (2), 261–277.
Mitchell, C., 1992. Industrial minerals laboratory manual: flake graphite. WG/92/30 British Geological Survey Technical Report. Mineralogy and Petrology Series.
Mudd, G., Josso, P., Shaw, R., Luce, A., Singh, N., Horn, S., Bide, T., Currie, D., Elliott, H., Grant, H., 2024. UK 2024 criticality assessment. British Geological Survey, Nottingham.
Natarajan, V., Porwal, N.K., Babu, Y., Rajeswari, B., Dhawale, B.A., Kumar, M., Godbole, S.V., Manchanda, V.K., 2010. Direct determination of metallic impurities in graphite by EDXRF. Appl. Radiat. Isot. 68 (6), 1128–1131.
Pacheco, F.E.R.C., Caxito, F.A., Pedrosa-Soares, A.C., Dussin, I.A., Gonçalves-Dias, T., 2021. Detrital zircon U-Pb and Lu-Hf data for a kinzigitic gneiss (Jequitinhonha Complex, Araçuaí Orogen, SE Brazil) constrain the age of a huge storage of Ediacaran carbon. J. South. Am. Earth Sci. 105, 102709.
Papike, J.J., Farmer, J., Bell, J.F., Morris, R.V., Klingelhöfer, G., Bernhardt, B., Schroeder, C., Gellert, R., Yen, A.S., McSween, H.Y., Rodionov, D.S., Squyres, S.W., 2006. Jarosite on Mars: a clue to acidic, aqueous conditions. Am. Mineral. 91 (5–6), 667–679.
Park, J., Cho, S.-J., Shin, S., Kim, R., Shin, D., Shin, Y., 2025. Overview of graphite supply chain and its challenges. Geosci. J. 29, 329–341.
Pedrosa-Soares, A.C., Babinski, M., Noce, C.M., Martins, M., Queiroga, G., Vilela, F.G., 2011. The Neoproterozoic Macaúbas Group, Araçuaí orogen, SE Brazil. Journal of South American Earth SciencesPereira, R., and Fragomeni, P. 2013. The graphite mineralization in the Aracoiába-Baturité District (CE): Geotectonic and metallogenetic implications. Brazilian J. Geol. 43, 223–234.
Pedrosa-Soares, A.C., Wiedemann-Leonardos, C.M., 2000. Evolution of sedimentary basins in eastern Brazil. J. South. Am. Earth Sci. 13 (1), 61–73.
Pope, N., Smith, P., 2023. Brazil's critical and strategic minerals in a changing world. Igarapé Institute.
Popova, A., 2017. Crystallographic analysis of graphite by X-ray diffraction. Coke Chem. 60, 361–365.
Powell, R., Holland, T.J.B., 2008. On thermobarometry. J. Metamorph. Geol. 26 (2), 155–179.
Robinson Jr, G.R., Hammarstrom, J.M., Olson, D.W., 2017. Graphite. *U.S.* Geological Survey Report, 1802J, Reston, VA.
Salzmann, C., Pellegrino, F., Hodoroaba, V.-D., 2024. STEM-in-SEM versus SE-InLens-type-SEM as a reliable analytical pair-tool for measurement of nanoparticle size and shape distribution. Microsc. Microanal. 30 (ement_1), ozae044.308. https://doi.org/10.1093/mam/ozae044.308.
Sandmann, D., Haser, S., Gutzmer, J., 2014. Characterisation of graphite by automated mineral liberation analysis. Mineral. Process. Extr. Metall. 123, 184–189.
Serviço Geológico do Brasil (SGB). 2026. An overview of critical and strategic minerals potential of Brazil: 2026 edition. CPRM (Serviço Geológico do Brasil), 1 PDF. ISBN 978-65-5664-722-7.
Silva, M.A., Pinto, C.P., Pinheiro, M.A.P., Marinho, M.S., Lombello, J.C., Pinho, J.M.M.P., Goulart, L.E., Magalhães, J.R., 2020. Mapa Geológico do Estado de Minas Gerais. CPRM, Belo Horizonte, Brazil.
Simandl, G.J., Paradis, S., Akam, C., 2015. Graphite deposit types, their origin, and economic significance. Br. Columbia Minist. Energy Mines Br. Columbia Geol. Surv. 3, 163–171.
Sousa, M.J.D., Matos, D.R., 2020. Projeto Avaliação do Potencial da Grafita no Brasil. Fase 1.
Spear, F.S., 1993. Metamorphic phase equilibria and pressure-temperature-time paths. Mineralogical Society of America, Washington, DC, USA.
Tetiker, S., Yalçın, H., Bozkaya, Ö., 2015. Approaches to the low grade metamorphic history of the Karakaya Complex by chlorite mineralogy and geochemistry. Minerals 5 (2), 221–246.
U.S. Geological Survey (2026) Mineral commodity summaries 2026: Graphite (natural). Available at: ⟨https://pubs.usgs.gov/periodicals/mcs2026/mcs2026-graphite.pdf⟩ (Accessed: 22 May 2026).
Wang, N., Liu, Y., Wang, L., Wang, H., Zhang, Y., Li, Y., Li, Y., Huang, Y., 2024. Innovative correlation relating the destruction of graphite flakes to the morphology characteristics of minerals. Physicochem. Probl. Mineral. Process. 60 (1).
Whitney, D.L., Evans, B.W., 2010. Abbreviations for names of rock-forming minerals. Am. Mineral. 95 (1), 185–187.
Zanin, M., Grano, S., Zhou, M., Skinner, W., 2019. The role of surface chemistry in the flotation of fine and coarse particles. Miner. Eng. 132, 149–159.
Zhao, Y., Liu, Y., Wang, L., Wang, H., Zhang, Y., Li, Y., Li, Y., Huang, Y., 2022. Graphite-based anode for high-energy lithium-ion batteries. Adv. Mater. 34 (3), 2106704.